Infrared spectroscopy of the Be/X-ray transient A0535+26

Mon. Not. R. Astron. Soc. 297, 657–666 (1998)

Infrared spectroscopy of the Be/X-ray transient A0535 + 26

J. S. Clark,[1] I. A. Steele,[2] M. J. Coe[1] and P. Roche[3]

[1]*Physics Department, University of Southampton, Southampton SO17 1BJ*
[2]*Astrophysics Research Institute, Liverpool John Moores University, Liverpool L3 3AF*
[3]*Astronomy Centre, MAPS, University of Sussex, Brighton BN1 9QH*

Accepted 1997 December 12. Received 1997 October 20; in original form 1996 December 18

ABSTRACT

We present infrared spectroscopy of the Be/X-ray binary HDE 245770/A0535 + 26 obtained over the period 1992–1995. The spectra show significant variability, reflecting changes in the circumstellar environment during this time. A reduction in the flux observed in the Paschen series lines between 1993 December and 1994 September correlates with a similar reduction in both the strength of Hα and the optical continuum emission, which can be attributed to a reduction in the emission measure of the disc. A turnover between optically thin and thick emission is seen for both Paschen and Brackett series lines, and allows an estimate of the disc density as $\sim 10^{12}$ cm^{-3}. Echelle spectroscopy reveals strong similarities between the He I 1.008, 2.058 μm, Hα and Paschen series line profiles, suggesting their formation in a similar (and asymmetric) region of the disc. In contrast, the line profile of He I 6678 Å indicates that it is formed at smaller radii than the other transitions.

Key words: binaries: close – stars: emission-line, Be – stars: individual: A0535 + 26 – stars: neutron – infrared: stars – X-rays: stars.

1 INTRODUCTION

The Be/X-ray binary system A0535 + 262 was discovered almost two decades ago, and due to its relative brightness and the well-known orbital period of the neutron star companion (111 d; Hayakawa 1981) it has been extensively studied. The system shows dramatic variability at all energies from X-rays to the infrared. The X-ray variability is described in detail by Motch et al. (1991), but can be briefly summarized as follows. X-ray outbursts of typically a few hundred milliCrab are normally seen at periastron, but two other types of behaviour are also observed: anomalous giant flares, and episodes where X-ray activity is absent during periastron. Prior to 1994, only three giant flares had been observed, in 1975, 1980 (Motch et al. 1991) and 1989 (Waters, private communication). Their onset demonstrates a delay with respect to periastron, and they typically reach 2–3 Crab intensity in the 2–20 keV range, a factor of 5–10 times greater than the flares that normally occur around periastron. Between 1992 and 1995 the system was observed to undergo all three types of behaviour at periastron, with a giant outburst occurring in 1994 February and March (Finger, Wilson & Hagedon 1994). Optical spectroscopy and optical and infrared photometry of the source during that same period are described in detail by Clark et al. (1998a,b). Here we merely plot Fig. 1, which shows the *V*-, *H*- and *K*-band light curves for the time over which observations were made.

Despite the interest in the system, and the extensive photometric and spectroscopic data base collected (Motch et al. 1991; Giovannelli & Graziati 1992), the system was not observed spectroscopically at infrared wavelengths until 1992, when we began a long-term monitoring campaign of the source using low-resolution grating spectra. In Section 2 we present the results from the first three years of that programme. Section 3 presents the results of single-epoch, high-resolution echelle observations of selected infrared lines in the system. In Section 4 we discuss the results of both programmes in terms of the necessary line-population mechanisms and locations of the line-forming regions. Finally, in Section 5 we give our conclusions.

2 LOW-RESOLUTION OBSERVATIONS

2.1 *I* (8400–8900 Å) band

I-band spectra were obtained using the 1-m Jacobus Kaptyn Telescope (JKT) on La Palma with the Richardson–Brearly spectrograph and the 1200 line mm^{-1} grating. Additional observations were made using the 1.5-m telescope of the

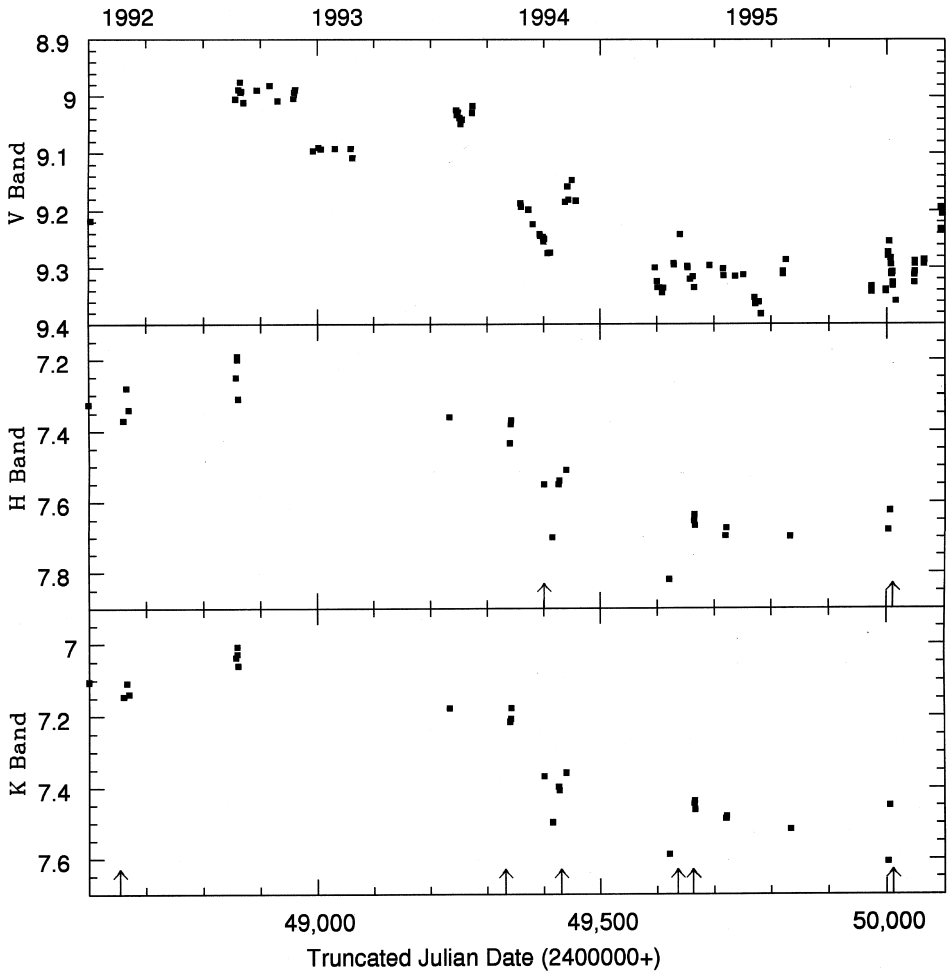

Figure 1. *V*-, *H*- and *K*-band light curves over the period of observation. The arrows denote spectroscopic observations.

Palomar Observatory equipped withu the *f*/8.75 Cassegrain-mode echelle spectrograph in regular grating mode. In both cases, data reduction was carried out using the Starlink-supported package FIGARO. The *I*-band spectra are plotted in Fig. 2.

Pa22 to Pa11 lines are clearly in emission on 1993 December 7, the lines appearing single-peaked, although asymmetric in comparison to the symmetrical single-peaked Hα profile from the previous night (Clark et al. 1998a). Substantial contamination of the Pa18 line by the O I 8446-Å line is seen. Contamination of Pa16, 15 and 13 is due to emission by calcium at 8498, 8542 and 8652 Å respectively from the 4^2P^0–3^2D triplet. A second *I*-band spectrum, obtained on 1994 September 17 with the same resolution, shows that the profiles have evolved into a double-peaked structure (also visible in Hα and Hβ). Equivalent widths from the 1994 September spectrum are $\sim$30 per cent lower than those from 1993 December (Table 1). Similarly, the Hα equivalent width between these dates also reveals a reduction of $\sim$40 per cent (Clark et al. 1998a).

2.2 *H* band

H- (and *K*-; see Section 2.3 below) band observations were made of the source using the CGS4 spectrometer of the UK Infrared Telescope, Mauna Kea, Hawaii during both service and scheduled time. The observations were made using both the short (150 mm) and long (300 mm) focal length cameras and the 75 line mm^{-1} grating. The standard CGS4 observing procedures were followed, with observations of standards at similar airmass to allow the removal of telluric features from the source spectra. The observations prior to 1994 were made using the 58×62 InSb array as a detector. Subsequent observations used the upgraded 256×256 array.

Initial data reduction was carried out at the telescope using CGS4DR (Puxley, Beard & Ramsey 1992). This removes bad-pixels, debiases, flat-fields, linearity-corrects and interleaves oversampled scan positions. The subsequent stages of data reduction (sky subtraction, extraction, deripppling, arc calibration and flux calibration) were carried out using the Starlink-supported packages FIGARO and DIPSO.

Two *H*-band spectra covering the H I Brackett series were obtained, the first on 1994 January 29, within a fortnight of the onset of the giant X-ray flare (see Section 1, and references therein), and the second 18 months after, on 1995 October 1 (Fig. 3). The Brackett series from Br11 to Br21 is in emission in both of the spectra taken (equivalent widths given in Table 2); the He I 1.7002-μm ($3p^3P^0$–$4d^3D$) line is also present in both spectra.

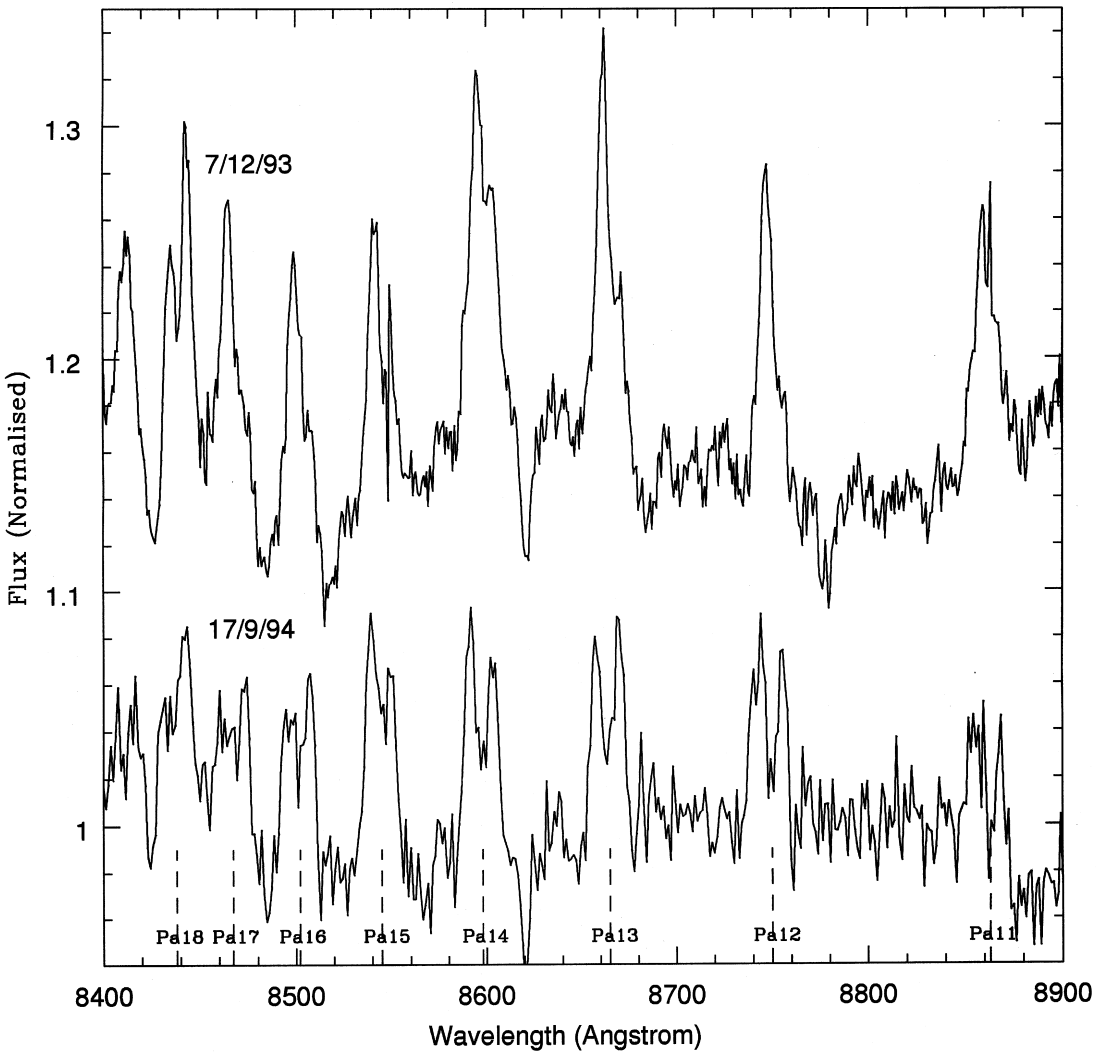

Figure 2. Observations of the Paschen series show it to be in emission before and after the decline in photometric luminosity.

Table 1. Equivalent widths (Å) for the Paschen series, and theoretical (the case B prediction of Storey & Hummer 1995 for $T_e = 20000$ K and $N_e = 10^{12}$ cm^{-3}) and observed line fluxes (errors estimated at ± 40 per cent; see text for details). The line fluxes are normalized to Pa17 in both spectra (absolute flux of 28.9×10^{-13} and 15.4×10^{-13} erg s^{-1} cm^{-2} for the 1993 December and 1994 September spectra respectively).

Line		7/12/93		17/9/94	
	Case B	EW	Flux	EW	Flux
Pa 11	3.80	1.4	1.50	0.9	2.25
Pa 12	2.97	1.4	1.35	1.1	2.14
Pa 13(+CaII)	2.33	1.8	1.57	1.3	2.25
Pa 14	1.88	2.2	1.68	1.3	1.98
Pa 15(+CaII)	1.51	1.4	1.22	1.4	2.16
Pa 16+(CaII)	1.23	1.5	1.13	1.0	1.48
Pa 17	1.0	1.5	1.0	0.8	1.0
Pa 18+(OI)	0.87	1.7	1.08	0.72	0.79
Pa 19	0.72	1.2	0.77	-	-
Pa 20	0.63	1.2	0.78	-	-

2.3 *K* band

K-band grating spectra were also obtained using CGS4 at UKIRT, and reduced using the same procedures outlined for the *H*-band spectra in Section 2.2. An additional spectrum was obtained from the Kitt Peak National Observatory 1.3-m telescope in 1994 September with the Cryogenic Infrared Spectrometer (CRSP). This spectrometer employs a 256×256 SBRC InSb array, and the spectrum was obtained with grating (150 line mm^{-1}) in second order, giving a 2.02 to 2.42 μm coverage with a resolution $\lambda/\Delta\lambda = 800$. Reduction was carried out with IRAF. Full details of the reduction process can be found in Hanson, Conti & Rilke (1996).

Seven low-resolution spectra were obtained in this region, and are shown in Fig. 4. All of the spectra show strong Brγ and 2.058-μm He I ($2s^1S$–$2p^1P^0$) emission. When observed, the Pfund series is also in emission. Due to their relatively low level, other He I features at 2.1120 μm ($3p^3P^0$–$4s^3S$) and 2.1132 μm ($3p^1P^0$–$4s^1S$) are hard to distinguish in

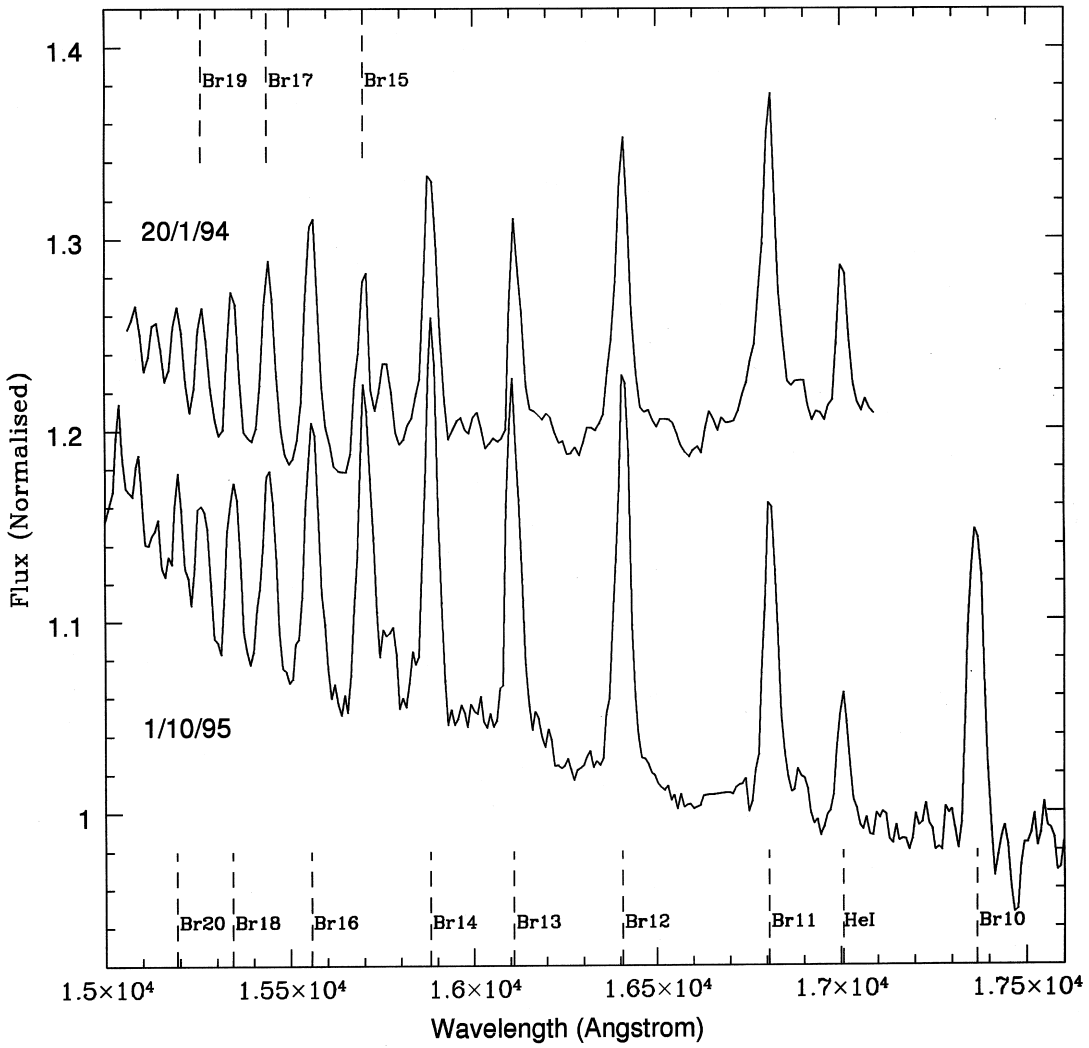

Figure 3. *H*-band observations show the Brackett series to be in emission.

Table 2. Equivalent widths (Å) for the Brackett series, and theoretical (case B) and observed line fluxes (errors estimated at ± 20 per cent; see text for details). The line fluxes have been normalized to Br17, for which the absolute fluxes on 1994 January 29 and 1995 October 1 are 8.8×10^{-13} and 8.0×10^{-13} erg s^{-1} cm^{-2} respectively.

Line		29/1/94		1/10/95	
	Case B	EW	Flux	EW	Flux
Br 11	4.80	7.8	1.55	7.8	1.45
Br 12	3.47	6.4	1.55	9.4	1.90
Br 13	2.59	4.6	1.10	7.5	1.60
Br 14	2.00	6.3	1.50	8.8	1.95
Br 15	1.57	5.0	1.20	7.6	1.70
Br 16	1.26	6.3	1.60	6.5	1.50
Br 17	1.0	3.9	1.00	4.2	1.00
Br 18	0.83	2.8	0.70	3.3	0.80
Br 19	0.71	2.2	0.65	2.3	0.55
Br 20	0.61	1.8	0.50	1.6	0.40

the pre-1994 (old array) spectra, but they are identifiable as being in emission from 1994 February onwards. Mg II 2.14 μm and Na I 2.21 μm are seen in emission in the 1994 October 8 and 1995 October 1 spectra.

3 HIGH-RESOLUTION OBSERVATIONS

Observations of selected emission features were made with the echelle grating of CGS4 on 1995 October 2. The basic reduction process for echelle data is similar to that outlined in Section 2 for grating data. However, the choice of standards for the removal of telluric features is a more difficult matter. From previous experience of low-resolution grating observations, early F dwarfs were chosen as standards. This was an attempt to compromise between having the strong hydrogen recombination lines that would result from an A-type standard and the large number of atomic and molecular features that contaminate G- and K-type standards. Division by these standards into the source spectra resulted

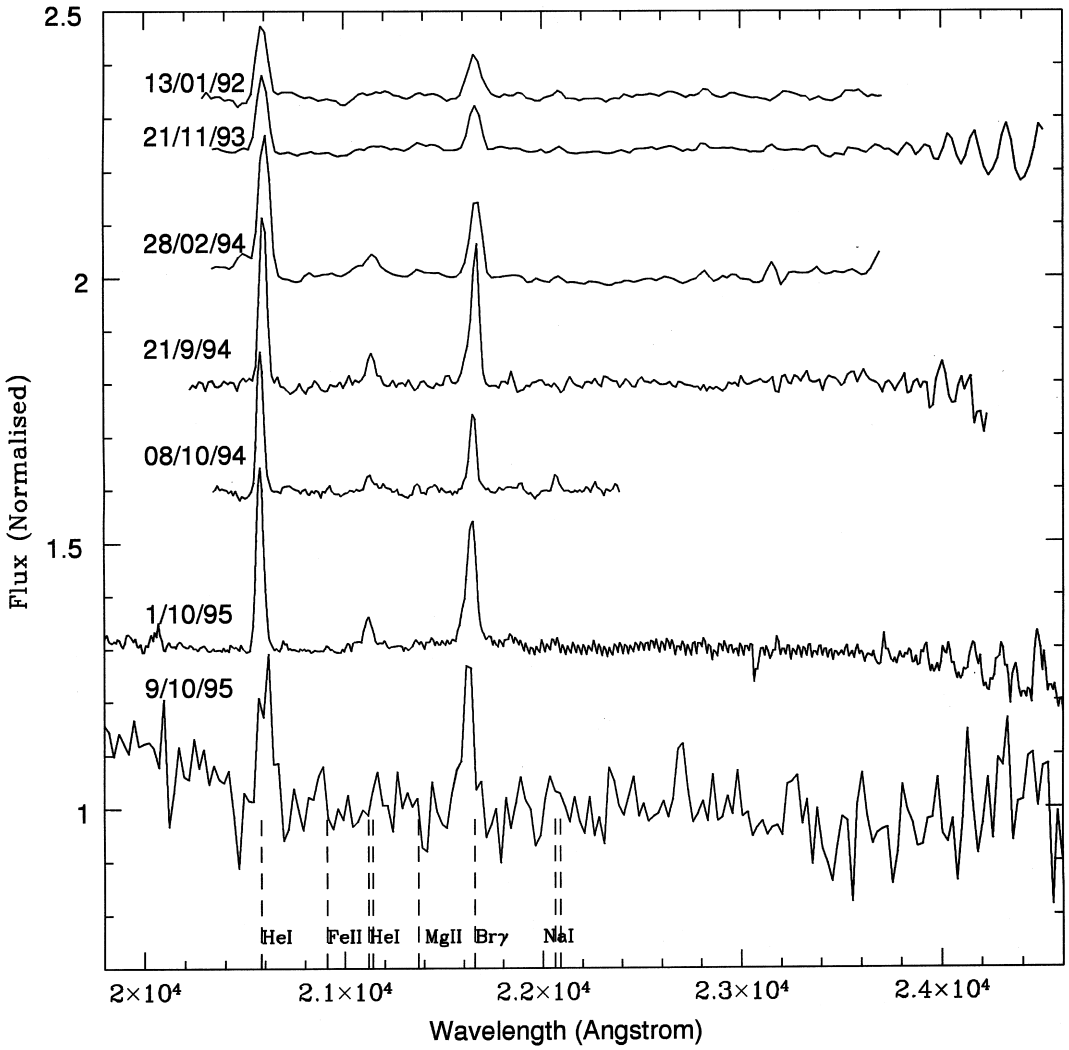

Figure 4. *K*-band observations taken over a 3-yr period show strong, variable H I and He II emission. Mg II 2.14 μm and Na I 2.21 μm is also seen in emission in the 1994 October 8 and 1993 October 1 spectra.

Table 3. Equivalent widths (Å) from *K*-band spectra (contemporaneous Hα observations are shown for comparison). Line fluxes also indicated; errors are estimated to be ±20 per cent.

Date	Brγ		He I 2.05		Date	Hα	
	EW	Flux	EW	Flux		EW	Flux
13/1/92	-6.7±0.2	6.0	-9.6±0.2	9.0	18/2/92	-10.8±0.2	600
21/11/93	-6.0±0.2	5.0	-9.5±0.2	10.0	5/12/93	-14.7±0.2	670
28/2/94	-11±0.2	6.0	-19.0±0.2	12.0	28/2/94	-9.1±0.2	500
21/09/94	-13±1	7.5	-15±1	9.5	9/9/94	-9.0±0.1	480
8/10/94	-6.5±0.2	4.0	-11.5±0.2	7.7	28/10/94	-7.7±0.1	430
1/10/95	-14.5±0.2	8.4	-14.5±0.2	9.0	16/10/95	-6.7±0.07	380
9/10/95	-14.0±2.0	8.2	-14.0±2.0	8.9	As above	As above	As above

in a number of spurious features (due to a large number of weak atomic and molecular lines in the spectra of the F dwarf standards); these were interpolated over in the spectra shown here.

Comparison of the equivalent widths obtained from the low-resolution (Table 3) and echelle spectra obtained on consecutive nights reveal discrepancies between the two data sets. It is likely that the systematic error is introduced in the reduction process due to the difficulty of interpolating over both the atmospheric water features and the underlying photospheric absorption line in the standard. Brγ is the least affected due to the lack of atmospheric water features present in that region of the spectrum, and also the strength of the absorption feature in the standard which makes it easy to remove. He I 2.058 μm is hard to reduce at low resolution (due to its position on a strong telluric edge), and

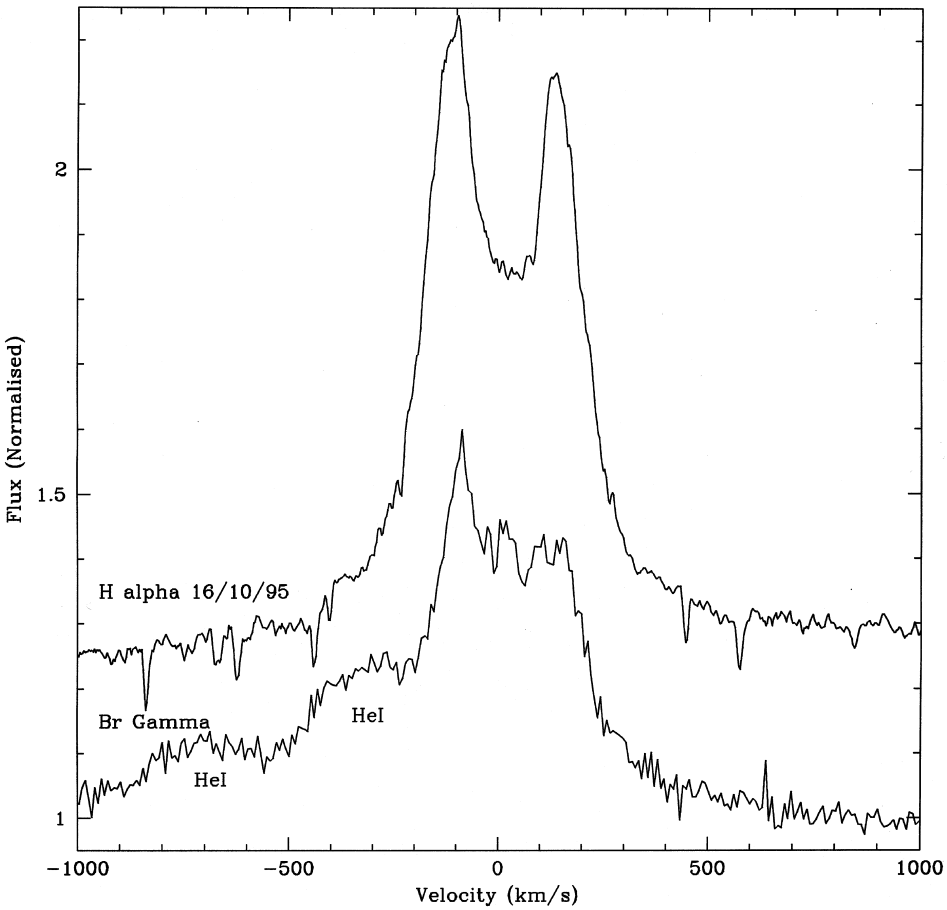

Figure 5. Resolved Brγ and Hα line profiles show the same asymmetry, probably due to the presence of a one-armed density wave.

thus it is likely that the echelle spectrum more accurately reflects the true equivalent width of the line. However, for consistency in our discussion of line fluxes in Section 4, *low-resolution* values will be used.

The high resolution enables the comparison of the line profiles to those of the optical lines observed quasi-simultaneously, and provides information on the relative position and kinematics of the emitting regions. It is apparent from Fig. 5 that there are two features in the blue wing of the Brγ profile, extending to projected velocities of $\sim$1000 km s^{-1}. These are most likely due to He I emission from lines at 2.1623 and 2.1653 μm. To try and quantify the effect of the contamination on the equivalent width, the line profile was fitted with two Gaussians centred on ~ -100 and $\sim +100$ km s^{-1}, thus excluding the He I emission, and the equivalent width was found to be 12.6 ± 0.4 Å, a decrease of $\sim$20 per cent over the value measured from the low-resolution spectrum taken on the same night. As is apparent from Fig. 5, both Hα and Brγ show a strong asymmetry, with the blue peak more strongly in emission. It is notable that the red peak visible in the Hα profile is much weaker in the Brγ spectrum. Emission in both spectra can be seen to extend out to projected velocities of $\sim$400 km s^{-1} (measurements for the blue wing are impossible for Brγ due to the contamination described above).

Two single He I lines were observed at high resolution, namely the 1.08- and 2.058-μm transitions. Both lines are shown in Fig. 6, with the Hα and He I 6678-Å profiles also shown for comparison (He I 6678 Å subject to a scaling factor of 5). It is immediately apparent that both He I profiles are similar to the Hα line profile. An additional component appears to be present in the blue wing of the He I 1.08-μm line, where a break in the line profile can clearly be seen at a projected velocity of -200 km s^{-1}. Due to the smoothing applied to the He I 2.058-μm line to remove contamination from the standard it is not clear whether the blue component is also present in this line. It is possible that it is also present in the Hα spectrum; however, the presence of a 'notch' in the spectrum due to a water vapour feature makes unambiguous identification difficult. Though double-peaked, the He I 6678-Å line differs from the two near-infrared lines, the central trough lying at the continuum level and the peak ratio differing from that of the infrared lines, with the red peak larger than the blue.

4 RESULTS

4.1 Line strengths

Sellgren & Smith (1992) demonstrated the effect of the optically thin/thick transition on hydrogen lines using 3.1–3.7 μm spectra of the Be star β Mon A. They were able to demonstrate that the higher H I transitions present fitted the optically thin, case B transition ratios, while Pfδ was

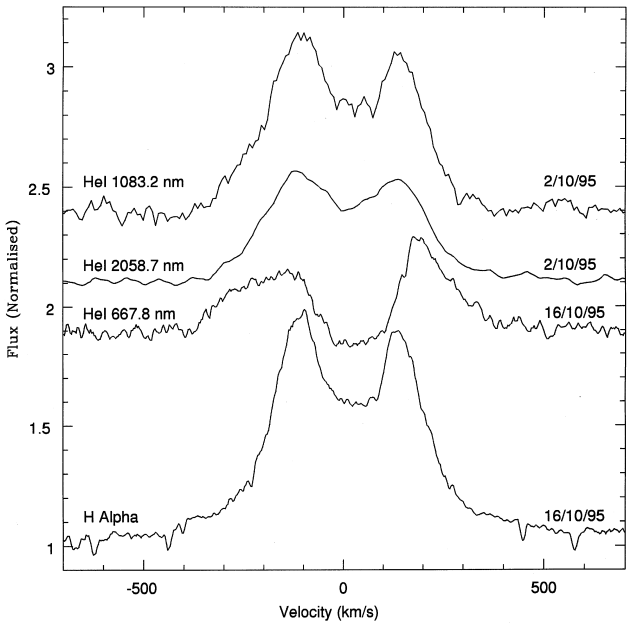

Figure 6. Resolved He I line profiles (Hα shown for comparison). He I 6678 Å plotted with a vertical exaggeration of 5.0 for clarity.

optically thick. We expect a similar transition between optically thin and thick emission will be seen in both the Paschen and Brackett series line fluxes (Hamann & Simon 1987).

To calculate the line fluxes, we measured equivalent widths of the hydrogen series lines in the spectra. These can be converted to line fluxes by multiplying by the continuum level adjacent to the line. This continuum is a combination of emission from the underlying B star and the circumstellar disc in the system.

To calculate this continuum, we employed the curve-of-growth model of Waters (1986). This requires knowledge of the underlying B-star continuum. This was obtained via a fit to a mean UV spectrum obtained from observations by *IUE* in 1994 February and September (Clark et al. 1998a). From these spectra, it was possible to obtain a best fit to the stellar emission, with a Kurucz model with $T=26\,000$ K, $\log g=3.5$ and $E(B-V)=0.72$ providing the best fit (consistent with Loore et al. 1984). The curve-of-growth model was normalized with respect to quasi-simultaneous (within 1 week) *UBVJHK* photometric data.

The measured emission-line fluxes were then corrected for underlying photospheric absorption using line fluxes from the Kurucz model spectrum. We note that work on LTE and NLTE models for stellar atmospheres (Murdoch, Drew & Anderson 1994) has shown that although LTE (Kurucz) models predict absorption for the infrared lines, NLTE effects can be sufficient to drive the lines partially into emission. Murdoch et al. (1994) suggest that the effect will be small for Brγ, and so we assume that our derived photospheric fluxes will not be substantially affected. In addition, we note that the low-resolution *K*-band spectra of O9.5 stars presented by Hanson et al. (1996) all show the Brγ and He I lines in absorption. Likewise, we note that in the high-resolution Brγ spectra of early-type stars presented by Zaal et al. (1997), the emission component due to NLTE processes is typically $\sim$10 per cent of the strength of the absorption profile. Finally, we note that the entire correction itself is small, due to the comparative weakness of the photospheric absorption profile (the Br11 photospheric line flux is predicted to be <15 per cent of the emission line). Overall, to allow for the uncertainties in photospheric line strength, and the flux derived from interpolation of the fit obtained via the curve of growth, we estimate an error of $\sim$20 per cent in our derived Brackett series line fluxes. The uncertainty associated with the Paschen series is larger ($\sim$40 per cent), due to the greater strength of the photospheric lines, and also the smaller continuum excess at shorter wavelengths. Nevertheless, we feel confident that the overall trend in line fluxes is real, since the Paschen series mirrors the behaviour of the Brackett series (Fig. 7).

Tables 1 and 2 therefore show our measured fluxes of the Brackett and Paschen lines, together with case B (optically thin) predictions (Storey & Hummer 1995). Both predicted and observed line fluxes have been normalized to Pa17, due to lack of contamination by other emission features. It should be noted that several Paschen lines (Pa13, 15, 16 and 18) are blended with other emission lines; it is therefore expected that the flux in these lines will depart from the predictions.

From Fig. 7 the Paschen series shows a turnover between optically thin and thick emission in all spectra, although due to the estimated errors, it is hard to constrain the position exactly. The line fluxes are consistent with optically thin emission from Pa20 to Pa14 in the 1993 December spectrum, and from Pa18 to Pa13 for the 1994 September spectrum, and optically thick emission is possible up to Pa15 for both spectra. Therefore the transition between optically thin and thick emission appears to lie between Pa15–14 and Pa15–13 for the 1993 December and 1994 September spectra respectively. Likewise, the Brackett series also show a transition between optically thin and thick emission; the observations are consistent with optically thin emission between Br20–Br16 and Br20–Br14 for the 1994 and 1995 spectra respectively. In both spectra optically thick emission is possible up to Br16, placing the turnover between Br17–15 for the 1994 January spectrum and Br17–13 for the 1995 October spectrum.

By considering the opacity factor for the last optically thin transition we can estimate the density of the emitting regions. The optical depth for a transition from n to n' may be calculated from the opacity factor $\Omega_{nn'}$ by the relationship

$$\tau_{nn'}=N_{\rm e}N_{+}\Omega_{nn'}L, \qquad (1)$$

where $N_{\rm e}$ and N_{+} are the densities of the electrons and recombining ions respectively, and L is the path-length in cm. For a given line to be optically thick ($\tau_{nn'}\sim1$) we will therefore require a certain minimum density and path-length. Now the opacity tables of Storey & Hummer (1995) show that the opacity factor for a given n decreases as n' increases. Therefore the n' at which the turnover occurs corresponds to that where the product in equation (1) is just insufficient to give an optical depth ~1. Assuming that $N_{\rm e}=N_{+}$ and that $\tau_{nn'}=1$ at the turnover, we can therefore estimate the electron density of the emitting region from

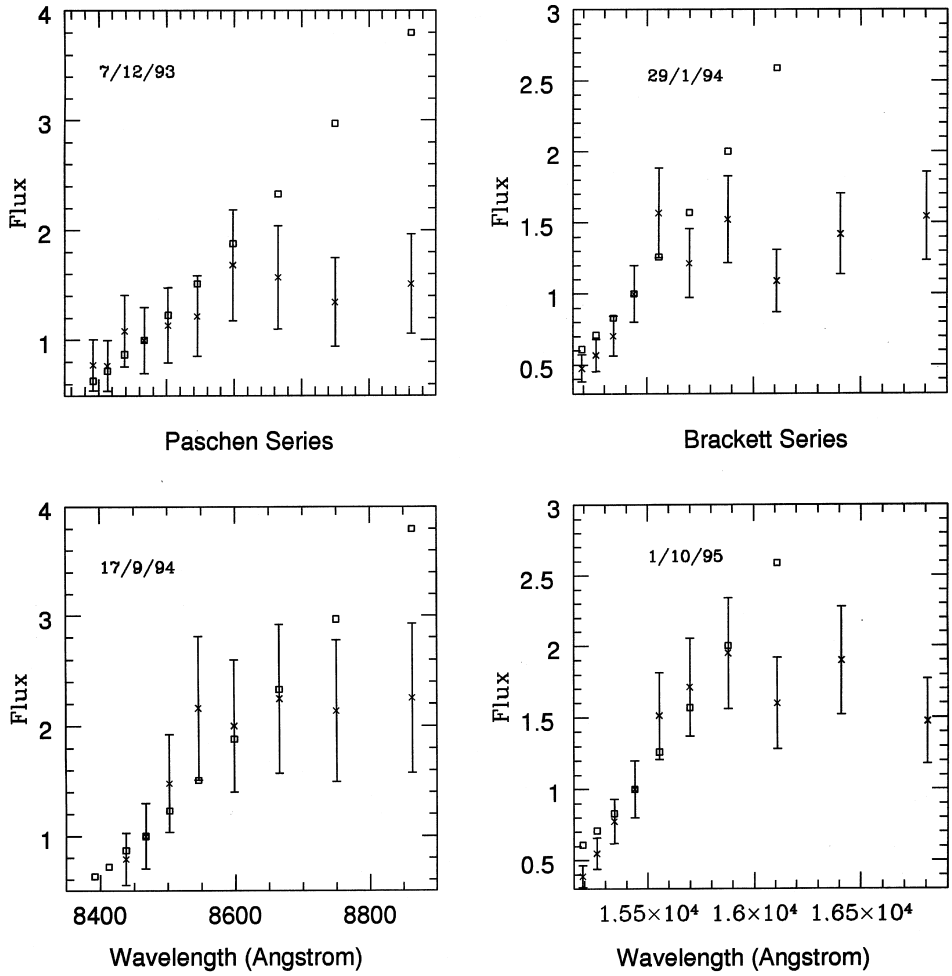

Figure 7. Comparison of theoretical case B predictions for the Paschen and Brackett series line fluxes (open squares) plotted against observed fluxes (where the fluxes are normalized to Pa17 and Br17 respectively). The transition between optically thin and thick emission is apparent.

$$N_e^2 = \frac{1}{\Omega_{nn'} L}. \quad (2)$$

To apply this procedure we require an estimate of the path-length of the emitting region. For moderate inclination angles this will be $\sim$the vertical height of the circumstellar disc. Observations of Be stars in shell-emission phases (Kogure, Hirata & Asada 1978; Pollitsch 1981) indicate a disc thickness of $\geq 1 R_{star}$ is necessary to account for the deep absorption cores. Models of disc formation involving rotation and stellar winds, however, predict a flattened disc of a smaller thickness (e.g., the wind-compressed disc model of Bjorkmann & Cassinelli 1993 predict a thickness of $< 0.2 R_{star}$). Combining these estimates indicates that the disc thickness lies in the range 0.2–$2 R_{star}$. For the $\sim$O9–B0 luminosity class III–V object we consider here this corresponds to a thickness (and hence L) of $\sim(0.15 - 1.5) \times 10^{12}$ cm (Allen 1973). Note that due to the form of equation (2) this factor of 10 uncertainty in L will correspond only to a factor of 3 uncertainty in the derived electron density.

For consistency we use the *lowest* possible turnover when applying the above method. By this criteria, the optical depth turnovers occur at Pa12 and Br13. We adopt a disc temperature $T = 20000$ K $\sim 0.8 T_{star}$. Using both the Paschen and Brackett turnover positions we therefore derive an upper limit to the density of the emitting regions of $N_e \sim 10^{12}$ cm^{-3}. The similarity of this value to other estimates of disc density in Be stars is encouraging (e.g., γ Cas by Scargle et al. 1978).

It should be noted that comparing the case B ratio between Pa11 and Pa20 ($\sim$6) to the observed ratio ($\sim$2), Pa11 would have to be some $\sim$3 times stronger than observed to be consistent with optically thin emission. It is therefore unlikely that errors introduced due to uncertainty in the strength of photospheric features could cause such an underestimate (indeed, if NLTE effects serve to drive the photospheric line partially into emission, the line flux would be overestimated).

We also note here that a comparison of the Pa17 line flux between the two spectra reveals a reduction by $\sim$50 per cent between 1993 December and 1994 September. Since this line is optically thin, its strength is proportional to the emission measure of the disc, and to the square root of the density (for constant volume). Note that we derived a simi-

lar decline in the disc emission measure from *UBV* photometry over the same period (Clark et al. 1998b).

4.2 Comparison of He I and Brγ line fluxes

The line flux ratio He I 2.058:Brγ for the source has varied between $\sim$1–2 over the period of the observations. This value is larger than might be expected if the He I-emitting region were constrained to lie very near the central object. However, in a parametric study of ψ Persei, Marlborough, Zijlstra & Waters (1997) calculated line strengths for optical and near-infrared hydrogen transitions for a wide variety of physical conditions. The degree of ionization in the disc is strongly dependent on the stellar radiation field, and in their model they ignore the envelope continuum emission and determine the degree of ionization from just the photospheric flux. With the accepted density behaviour for Be star discs (i.e., a rapidly falling disc density with increasing radius) the degree of ionization will actually *increase* with radius, since the disc density will fall more rapidly than the photospheric flux (due to geometrical dilution). Hence material at large radii can also contribute to the He I 2058- and 1.083-μm lines, so a much higher flux is seen in comparison to the Brγ line than might be expected. Marlborough et al. show that the weaker infrared transitions will be formed at smaller radii than Hα, due to a combination of the reduction of the source (Planck) function at large radii, and an increase in opacity with radius. Consequently, we might expect both differences in the behaviour of the profile and strength of Brγ compared to Hα, since Hα will be influenced much more strongly than Brγ by conditions in the outer disc. This is seen both in the variability of the Brγ:Hα flux ratio, and in the differences in the line profiles (Section 4.2).

4.3 Line profiles

Since thermal broadening will contribute only $\sim$10 km s^{-1} to the width of the line, Doppler broadening is expected to be the dominant process in the line profiles, which therefore provide a diagnostic of velocities within the disc. Unfortunately, our Paschen series spectra are of relatively low resolution and signal-to-noise ratio; however, in gross physical characteristics, they closely resemble Hα, with a transition between single- and double-peaked emission visible in both spectra. The overall symmetry of both sets of spectra strongly argues for predominantly rotational motion within the disc, with little or no component of radial velocity, the asymmetries apparent in Hα being explained by the presence of a global one-armed oscillation within the disc (Clark et al. 1998a).

The similarity of the He I 2.058- and 1.08-μm lines to the Hα profile is immediately apparent. The He I 2.058- and 1.083-μm lines are the triplet and singlet 2P–2S transitions, and so are similar in location in the He I energy diagram. Thus we might also expect them to have similar profiles. The similarity with Hα reflects the fact that they are all relatively strong transitions and are populated via recombination. It might therefore be expected that they arise in coincident regions of the disc.

He I 6678 Å is a weaker transition, and hence is likely to be formed at smaller radii. The different profile (with an opposite V/R ratio to the infrared helium lines and Hα) reflects this.

Brγ is expected to form as an intermediate case between these two extremes, being produced in a region smaller than Hα but larger than He I 6678 Å. Thus the profile still demonstrates the gross characteristics of the Hα profile (i.e., asymmetry due to the presence of a global one-armed disc oscillation confined in the inner regions of the disc), but with a larger degree of asymmetry, due to radial dependence of both the rotational velocity, and also the one-armed density wave.

5 CONCLUSIONS

We have presented both low- and high-resolution infrared spectroscopy of the Be/X-ray binary HDE 245770/A0535+26 obtained over the period 1992–1995. The spectra show significant variability over the period, reflecting changes in the circumstellar environment during this time.

Paschen, Brackett and Pfund series are all seen to be in emission, and the Paschen and Brackett series are seen to demonstrate a transition from optically thin to thick behaviour. Estimates of the disc density based on the position of the turnover indicate a density of the order of $N_e = 10^{12}$ cm^{-3}, consistent with estimates of disc density in Be star systems from other sources.

A reduction in the flux observed in the Paschen series lines between 1993 December and 1994 September correlates with a similar reduction in both the strength of Hα and the optical continuum emission, which can be attributed to a reduction in the emission measure of the disc over that period, a result confirmed by analysis of the optically thin *UBV* continuum.

Echelle spectroscopy reveals strong similarities between the He I 1.008, 2.058 μm, Hα and Paschen series line profiles, suggesting their formation in a similar (and asymmetric) region of the disc. In contrast, the line profile of He I 6678 Å indicates that it is formed at smaller radii than the other transitions. Brγ appears to be formed between these two regions.

ACKNOWLEDGMENTS

We thank PATT for their support of the long-term monitoring campaign. UKIRT is run by the JAC, Hawaii on behalf of the UK PPARC. We especially thank the UKIRT support staff for their assistance in obtaining many of the observations presented here. The work was carried out partly with Starlink hardware and software. The files containing the opacity information were obtained from the NASA Astronomical Data Centre. JSC wishes to acknowledge a PPARC studentship award. We thank C. Everall for his help in obtaining the early observations. Finally, we also thank the referee for many helpful comments that resulted in substantial improvements to the paper.

REFERENCES

Allen C. W., 1973, Astrophysical Quantities, 3rd Ed., Athlone Press

Bjorkmann J. E., Casinelli J. P., 1993, ApJ, 409, 429
Clark J. S. et al., 1998a, MNRAS, 294, 165
Clark J. S. et al., 1998b, MNRAS, submitted
de Loore C et al., 1984, A&A, 141, 279
Finger M. H., Wilson R. B., Hagedon K. S., 1994, IAU Circ. 5931
Giovannelli F., Graziati L. S., 1992, Space Sci. Rev., 59, 1
Hamann F., Simon M., 1987, ApJ, 318, 356
Hanson M. M., Conti P. S., Rilke M. J., 1996, ApJS, 107, 281
Hayakawa S., 1981, Space Sci. Rev., 29, 221
Kogure T., Hirata R., Asada Y., 1978, PASJ, 30, 385
Marlborough J. M., Zijlstra J.-W., Waters L. B. F. M., 1997, A&A, 321, 867
Motch C., Stella L., Janot-Pacheco E., Mouchet M., 1991, ApJ, 369, 490
Murdoch K. A., Drew J. E., Anderson L. S., 1994, A&A, 284, L27
Pollitsch G. F., 1981, A&A, 97, 175
Puxley P. J., Beard S. M., Ramsey S. K., 1992, in Grosbul P., ed., Proc. 4th ESO/ST-ECF Data Analysis Workshop
Scargle J. D. et al., 1978, ApJ, 224, 527
Sellgren K., Smith R. G., 1992, ApJ, 388, 178
Storey P. J., Hummer D. G., 1995, MNRAS, 272, 41
Waters L. B. F. M., 1986, A&A, 162, 121
Zaal P. A., Waters L. B. F. M., Geballe T. R., Marlborough J. M., 1997, A&A, 326, 237